34th Annual International Conference of the IEEE EMBS
San Diego, California USA, 28 August - 1 September, 2012

# Characterization of Fractionated Electrograms Using a Novel Time-frequency Based Algorithm

Behnaz Ghoraani, Sridhar Krishnan, Vijay S. Chauhan *(MD)*

***Abstract*— Atrial fibrillation (AF) arises from complex spatiotemporal atrial activation. Current treatment for patients with AF when antiarrhythmic drugs have failed is catheter ablation which uses Radiofrequency (RF) energy to destroy heart tissues that drive AF. Therefore, AF can be terminated once the AF source is localized and eliminated by RF ablation. There is considerable interest in defining whether complex fractionated atrial electrograms (CFAE) indicate AF-perpetuation sites. This work proposes a novel time-frequency (TF) based algorithm to characterize CFAE electrograms (EGMs). The proposed technique obtains an automated classifier that is trained based on the differences evidenced between the TF structures of CFAE and non-CFAE EGMs. These characteristics are quantified using 5 TF features which are extracted using a TF matrix decomposition method performed on the EGM. The results from 5 patients with AF show that the proposed method is successful in identifying CFAE vs. non-CFAE EGMs, and might open new perspectives for a novel and reliable mapping technique to accurately characterize and understand AF mechanism.**

## I. Introduction

Atrial fibrillation (AF) is the most common, abnormal rhythm of the heart that can cause significant morbidity including heart failure, stroke and increase mortality. Great strides have been performed in understanding the initiation and continuation of AF, and localizing the AF trigger sites; however, the mechanisms sustaining the AF is far less clear. *In vivo* AF mapping studies in humans have proposed two hypothesis for maintenance of AF: dominant frequencies (DF) [1] and complex fractionated atrial electrograms (CFAE) [2]. DF mapping is predicted on the hypothesis that finding the highest frequency activation sites will identify focal drivers for AF, while CFAE mapping attempts to find sites manifesting short cycle length activities that may perpetuate AF. Ablating at CFAE sites has demonstrated contradictory success rates in improving AF ablation, while AF sources consistent with high DF sites have mainly shown in animal studies such optically mapped sheep AF. In terms of signal analysis techniques, a spectral approach has been proposed to estimate the DF of the EGM [3], and temporal analysis and algorithms have been suggested to localize CFAE regions [2]. However, the accuracy and efficiency of these techniques in identifying clinically relevant AF sources remains controversial.

Behnaz Ghoraani and Vijay S. Chauhan are with Division of Cardiology, University Health Network, Toronto, ON, Canada, M5G 2C4, vijay.chauhan@uhn.on.ca

Sridhar Krishnan is with Department of Electrical and Computer Engineering, Ryerson University, Toronto, ON, Canada, M5B 2K3, krishnan@ee.ryerson.ca

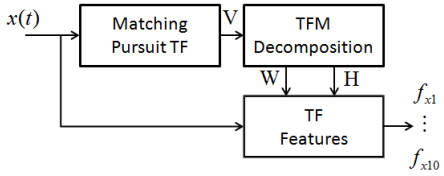


Fig. 1. Schematic of the proposed TF feature extraction method for CFAE identification. Ten feature vectors are extracted from each EGM ($x(t)$), and each vector includes 5 values.

The pathophysiology of CFAE is not well defined. Although some CFAE indicate critical substrate based on intraoperative human AF mapping studies, catheter ablation of CFAE sites has demonstrated only 30-50% freedom from AF at 1st year. The present study proposes a novel and reliable signal analysis technique to characterize CFAE EGMs which are associated with AF maintenance sources in order to localize driver sites in patients prior to ablation, and therefore, improve the success rate of the procedure. In this paper, we propose a spectral-temporal based algorithm to localize CFAE from the intracardiac signals collected from the left atrium during *In vivo* AF mapping. This method is based on time-frequency (TF) matrix decomposition method proposed by our group in order to quantify ECG signals to predict sudden cardiac death risk. We employ this TF technique to accurately characterize CFAE in order to detect these clinically important regions in the left atrium.

## II. Methods

As shown in Fig. 1, the proposed TF feature extraction algorithm consists of three stages: TF representation, TF matrix decomposition, and TF feature extraction.

### A. TF Representation

Matching pursuit (MP) TF representation was used to build the TF domain (TFD) of EGMs. MP decomposes a signal, $x(t)$, into a linear combination of TF functions $G_{\gamma_i}(t)$ selected from a redundant Gabor dictionary of TF basis functions [4]. Once MP selects the collection of TF atoms that model the signal $x(t)$, MP-TFD of the given signal, $\mathbf{V}(t,f)$, is constructed by summing up the TFD of each decomposed TF atom as shown below:

$$\mathbf{V}(f,t) = \sum_{i=1}^{I} |a_{\gamma_i}|^2 \, \mathbf{WVG}_{\gamma_i}(f,t) \qquad (1)$$

where $\mathbf{WVG}_{\gamma_i}(f,t)$ is the Wigner-Ville distribution of the Gabor atom $G_{\gamma_i}(t)$, and $I$ is the number of selected atoms.

The MP decomposition with Gabor TF atoms has been chosen in this study because of its superior TF resolution [5], cross-term free nature, adaptively, and suitability for pattern recognition applications. It should also be mentioned that EGMs may contain both Gabor and non-Gabor structures. However, the non-Gabor structures are generally random and noise-like, without definite TF function. If a non-Gabor structure does belong to the EGM structure, and does not correlate with any of the TF functions in the Gabor dictionary, it is broken into smaller structures each diluted over many functions leading to non-sparse representation [4].

### B. TF Matrix Decomposition

Non-negative matrix factorization (NMF) is applied to the TF matrix in such a way that the TF matrix is decomposed into two sets of vectors denoted with $\{w_1, w_2, ..., w_r\}$ and $\left\{h_1^T, h_2^T, ..., h_r^T\right\}$, where $r$ is the number of factors, $w_i$ and $h_i^T$ represent the spectral and temporal structure of each component, respectively. We arrange each vector set into two matrices **W** and **H** *base* and *coefficient* matrices, respectively. The relationship between the decomposed TF matrices and the original TF matrix can be shown as follows:

$$\begin{aligned} \mathbf{V}_{M\times N}(f,t) &= \mathbf{W}_{M\times r}\mathbf{H}_{r\times N}, \\ &= \textstyle\sum_{i=1}^{r}\{w_{fi}h_{it}\}, \end{aligned} \tag{2}$$

where $w_{fi}$ and $h_{it}$ are the elements of base and coefficient matrices, respectively.

### C. TF Feature Extraction

Five TF features are extracted from each base component and the corresponding coefficient vector: $\mathrm{S}_W$, $\mathrm{S}_H$, $\mathrm{D}_W$, $\mathrm{D}_H$, and $\mathrm{MO}_W$.

*1) Sparsity:* For each base and coefficient vector, we extract two sparsity features as explained below:

$$\mathrm{S}_{w_i} = \frac{\sqrt{M} - \left(\sum_{m=1}^{M} w_i(m)\right) / \sqrt{\sum_{m=1}^{M} w_i^2(m)}}{\sqrt{M}-1}, \tag{3}$$

$$\mathrm{S}_{h_i} = \frac{\sqrt{N} - \left(\sum_{n=1}^{N} h_i(n)\right) / \sqrt{\sum_{n=1}^{N} h_i^2}}{\sqrt{N}-1}, \tag{4}$$

This function is unity if and only if the vector contains a single non-zero component, and is zero if and only if all the components are equal. For non-CFAE EGMs we expect to have higher spectral sparsity features (i.e., $\mathrm{S}_W$) and lower temporal sparsity features (i.e., $\mathrm{S}_H$), while CFAE ones have lower spectral and higher temporal sparsity values.

*2) Sum of derivative:* This feature captures the discontinuities and abrupt changes in the EGM:

$$\mathrm{D}_{w_i} = \sum_{m=1}^{M-1} w_i'(m)^2, \tag{5}$$

where

$$w_i'(m) = w_i(m+1) - w_i(m),\ m = 1, ..., M-1, \tag{6}$$

and

$$\mathrm{D}_{h_i} = \sum_{n=1}^{N-1} h_i'(n)^2, \tag{7}$$

where

$$h_i'(n) = h_i(n+1) - h_i(n),\ n = 1, ..., N-1, \tag{8}$$

In these features, first, we calculate the derivative of the vector, and then use the sum of the derivative vector as one of the features. This feature is small if there is a uniform structure in the vector (i.e., spectral components in non-CFAE); otherwise, it is a large value.

*3) Moments:* The first moment of each base vector, $\{w_i\}_{i=1,...,r}$, is extracted as shown below:

$$\mathrm{MO}w_i = \sum_{m=1}^{M} m w_i(m), \tag{9}$$

where $\mathrm{MO}w_i$ is the spectral moment.

## III. Experimental Assessment

In 5 patients with AF (2 paroxysmal, 3 persistent), bipolar EGMs were recorded from the endocardial surface of the left atrium using a 20 electrode circular mapping catheter (Lasso, Biosense Webster) before AF ablation. The 20 electrodes are paired with 6mm spacing between electrode pairs, and are evenly distributed around the circumference of the catheter, which has a variable diameter of 15-25mm. Approximately 30 sites in the left atrium were sampled by roving the circular mapping catheter within the chamber, and AF was recorded for 2.5 seconds at each site at a sampling frequency of 1kHz. CFAEs were visually identified if bipolar recordings contained fractionated EGMs with two deflections or more, and/or have a perturbation of the baseline with continuous deflection of a prolonged activation complex and duration >50 ms, and a very short cycle length (<120 ms) [2].

Figs. 2 and 3 display two EGMs with non-CFAE and CFAE characteristics, respectively. The frequency and temporal resolution of the TF representation is 512 and 2,500 samples, respectively (i.e., $M = 512$ and $N = 2500$). It can be seen in Fig. 2.A that the non-CFAE signal contains noncomplex and clearly separable AF activations, while the CFAE EGM (Fig. 3.A) is complex and fractioned over the 2.5 second. The proposed TF method is applied to both signals and the decomposed spectral and temporal components are shown in Figs. 2.C-D and 3.C-D. A value of 10 is experimentally decided to be a suitable choice for the number of factor (i.e., $r = 10$). Three different structures were observed in the decomposed components: (i) Wideband: the spectral energy is spread over frequency domain (e.g., component 2 in Fig. 2.C). (ii) Narrowband: the spectral energy contains a narrow range in the frequency domain (e.g., component 4 in Fig. 3.C). (iii) Multicomponent: there are two narrwoband energy contents (e.g., component 6 in Fig. 3.C). It can be seen that the spectral components in non-CFAE EGM are more wideband, while the ones in CFAE signal are more narrowband and multicomponent. This observation could be predicted as the activations in non-CFAE EGMs are steep deflections which result in wideband components, while the CFAE contains more sinusoidal structures with narrowband or multicomponent contents. We have used our proposed

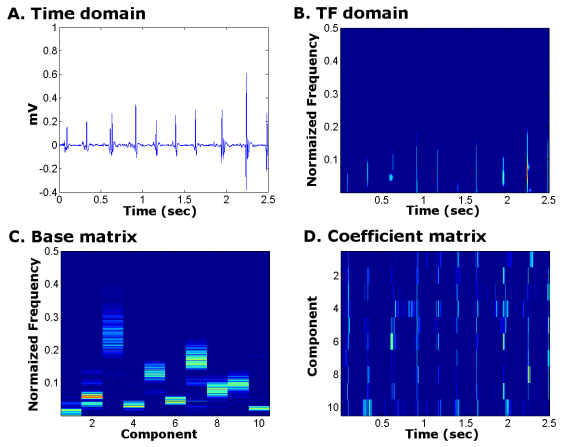


Fig. 2. A Non-CFAE EGM has been decomposed into spectral and temporal components using the proposed TF algorithm. A: Electrogram. B: TFD obtained using MP-TF algorithm (see Section II-A). C and D: Base (i.e., spectral components) and coefficient (i.e., temporal components) matrices decomposed from the TFD (see Section II-B), respectively.

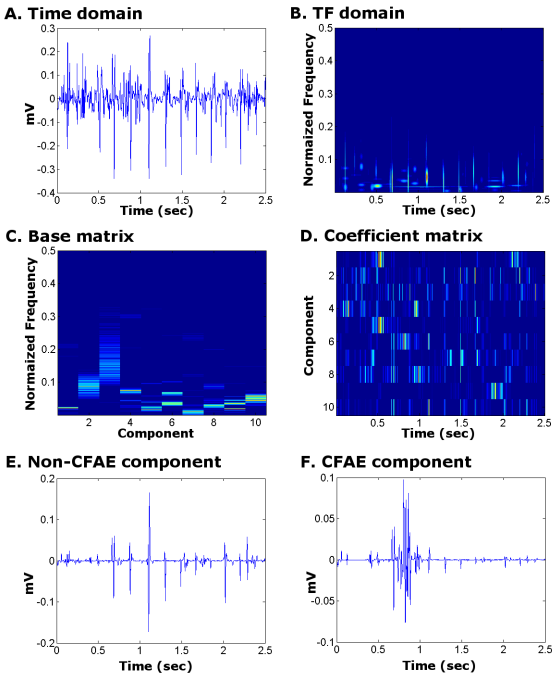


Fig. 3. A CFAE EGM has been decomposed into spectral and temporal components using the proposed TF algorithm. A: Electrogram. B: TFD obtained using MP-TF algorithm (see Section II-A). C and D: Base (i.e., spectral components) and coefficient (i.e., temporal components) matrices decomposed from the TFD (see Section II-B), respectively. E and F: The time domain representation of components 3 and 6, respectively.

TF feature extraction method to quantify this property of non-CFAE and CFAE EGMs in order to detect CFAE sites in the left atrium. The proposed TF features are extracted from each decomposed matrices as explained in Section II-C. Fig. 4 shows the obtained features for the two EGMs in Figs. 2.A and 3.A. There are three clusters of features: non-CFAE cluster (i.e., C1), CFAE cluster (i.e., C2), and joint CFAE and non-CFAE cluster (C3). Because of the difference between the structures of the two EGMs, feature vectors from the wideband components with organized temporal structure were located far from the CFAE features which are associated to narrowband or multicomponent with disorganized behaviour in time. The joint cluster is the result of low-frequency structure of the AF activation morphology (e.g., components 1 and 10 in Fig. 2.C and components 1, 5, and 7 in Fig. 3.C) and should be discriminated from the other two clusters so that these features do not affect the final decision making. We have used the aforementioned difference between the non-CFAE and CFAE EGMs to train a classifier which can be further used to identify fractionated EGMs. Three classes are assumed in this work: clusters dedicated to non-CFAE features, CFAE feature, or joint non-CFAE and CFAE features.

The classification method applied in this work consists of two stages. In the first stage, the Self Organizing Tree Map (SOTM) algorithm is run on the train data to obtain the cluster centers. Since the formation of the clusters is based on the representation of the data to the SOTM network, some of the clusters might not be valid and thus clusters with small number of samples are eliminated. A membership matrix is then calculated at this stage based on the distribution of each class in different clusters. Each entry in the membership matrix, $m_{ij}$ (which we call a membership coefficient) indicates the probability of a vector in the cluster $i$ to belong to the $j$th class.

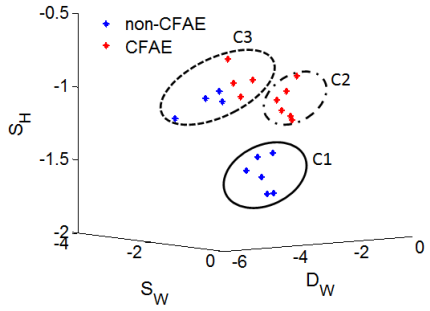


Fig. 4. The EGMs in Figs. 2 and 3 are shown in the feature domain. C1: A cluster with non-CFAE features. C2: A cluster with CFAE features. C3: A cluster with joint non-CFAE and CFAE features.

$$M = \begin{bmatrix} m_{11} & m_{12} \\ m_{21} & m_{22} \\ \vdots & \vdots \\ m_{C1} & m_{C2} \end{bmatrix} \tag{10}$$

where

$$m_{ij} = p(\theta_j | C_i) \tag{11}$$

These coefficients will be used in calculation of the membership degree for each of the test vectors. The main advantage of calculating the membership coefficients is to take into consideration the overlap of the CFAE and non-CFAE classes in the feature space. When a signal is projected onto the

TABLE I

CLASSIFICATION RESULT. GOLD STANDARD: VISUAL INSPECTION [2].

| | Method | Class | Gold Standard | |
|---|---|---|---|---|
| | | | CFAE | Non-CFAE |
| Test | TF features | CFAE | 100% | 0% |
| | | Non-CFAE | 0.8% | 99.2% |
| | ICL | CFAE | 83% | 17% |
| | | Non-CFAE | 0% | 100% |

feature space, some of its representing vectors may fall in the areas which are common within two or more classes. By using this approach, less weight is associated with the vectors that are located in the overlap area. In the second stage, each of the feature vectors representing a test signal is assigned to one the cluster centers found in the previous stage based on the minimum Euclidean distance criterion. For each signal the scatter vector, $S$ is defined as

$$S = [s_1, s_2, ..., s_c] \tag{12}$$

where $s_i$ is the number of the representing vectors for a test signal that fall within th $i_{th}$ cluster and C is the number of clusters. Finally the probability of a signal belonging to a non-CFAE or CFAE class is calculated according to the distribution of its representing feature vectors in different clusters and can be described as $\Phi(j) = S.M(j)$, and the signal is labeled to belong to the class associated with the maximum value of $\Phi(j)$.

We studied 5 patients with AF and identified CFAE EGMs using the proposed method. The identification results are shown in Table I. Also, CFAE was identified using interval confidence level (ICL) as have been utilized in a programmable software (CFAE Software Module, Biosense Webster) which provides online automated identification display of CFAEs during ablation procedure. ICL [6], defined as the number of intervals between consecutive CFAE complexes during 2.5 second recordings, and the CFAE sites with an ICL $\geq$7 were considered as sites with highly repetitive CFAEs, which are thought to be potential ablation targets. The classification results in Table I demonstrates that the proposed TF feature extraction and classification successfully localizes the CFAE EGMs with 99.2% accuracy (i.e. sensitivity = 99.2%and specificity = 100%). This method offers a significant improvement over ICL algorithm (i.e., sensitivity = 100%and specificity = 85%). The proposed method is more accurate in rejecting the EGMs with no true CFAE structure. As a result, the ablation procedure could be led to real CFAE sites and potentially improve the success rate and reduce the procedure time. Fig. 5.A demonstrates a case where the ICL method reports an EGM with a high frequency activation (i.e., DF = 9.2 Hz) as a CFAE source, while the proposed method correctly identifies that the EGM is a non-CFAE site. An example of an electrogam with high DF content (i.e., DF = 8.8 Hz) which both the proposed and ICL algorithms are successful in identification of the CFAE site is displayed Fig. 5.B.

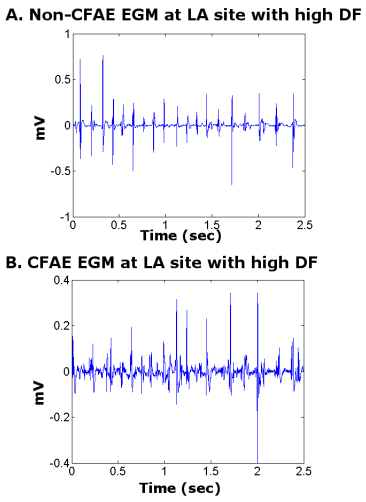


Fig. 5. A case of discordance between the proposed TF method and the conventional ICL. While B is correctly classified as CFAE using both method, only the proposed TF method successfully identifies the EGM in A as a non-CFAE site.

## IV. CONCLUSION

In this study, we introduced a novel TF based approach for the identification of CFAE sites, based on TF feature extraction and classification. This approach builds the TF representation of the EGMs collected from the left atrium, and decomposes the TFD into its underlying spectral and temporal components. It was shown that the decomposed spectral and temporal vectors show a different behaviour in case of CFAE or non-CFAE EGMs. This observation provided a motivation to extract five TF features from these vectors, and use them for the purpose of localization of CAFE EGMs. This method was performed on a dataset collected from 5 AF patients, and exhibited an improved success rate over the existing automated algorithms for CFAE detection. The presented algorithm provided a more accurate approach to locate CFAE sites. The integration of this method along with DF mapping may lead to successful identification of critical arrhythmic sites which are potentially arise from AF sources, and thereby, leading to a customized AF ablation procedure with a high success rate.

## REFERENCES


[1] P. Sanders, O. Berenfeld, M. Hocini, and et al., "Spectral analysis identifies sites of high-frequency activity maintaining atrial fibrillation in humans," *Circulation*, vol. 112, pp. 789 – 797, 2005.

[2] K. Nademanee, J. McKenzie, E. Kosar, and et al., "A new approach for catheter ablation of atrial fibrillation: mapping of the electrophysiologic substrate," *JACC*, vol. 43, pp. 2044 – 2053, 2004.

[3] G. Botteron and J. Smith, "A technique for measurement of the extent of spatial organization of atrial activation during atrial fibrillation in the intact human heart," *IEEE Trans on Biomed Eng*, pp. 579 – 586, 1995.

[4] S. G. Mallat and Z. Zhifeng, "Matching pursuits with time-frequency dictionaries," *IEEE Trans on Signal Proc.*, vol. 41, pp. 3397–3415, 1993.

[5] L. Cohen, "Time-frequency distributions – a review," *Proc of the IEEE*, vol. 77, pp. 941–981, 1989.

[6] D. Scherr and et al., "Automated detection and characterization of complex fractionated atrial electrograms in human left atrium during atrial fibrillation," *Heart rhythm*, vol. 4(8), pp. 1013 – 1020, 2004.